

NUMERICAL MODELING OF SHEET AND TIP VORTEX CAVITATION WITH FLUENT 5

Gotfred S. Berntsen
NTNU, ITEV
N7491 Trondheim, Norway

Morten Kjeldsen
NTNU, ITEV
N7491 Trondheim, Norway

Roger E. A. Arndt
University of Minnesota
Mississippi River@3rd AVE SE
Minneapolis, MN 55414

Abstract

This paper presents numerical work made with the commercial CFD code Fluent 5 by Fluent Inc. The main investigation constitutes a 2D NACA 0015 hydrofoil grid. The grid is designed to resemble a physical setup found at Saint Anthony Falls Laboratory (SAFL) in Minneapolis, MN, USA. The study is done for cavitation numbers ranging from inception to supercavitating at two different angles of attack. All numerical results are compared to corresponding experimental results from the SAFL tunnel in a quantitative manner. The general characteristics of the cavitating flow was very well predicted. Especially, the cavity length is calculated with high accuracy. Lift variations as a function of cavitation number are also reasonably well predicted. The current model, however, seems to have problems with the dynamics of the system.

The next section presents a 3D calculation on a NACA 66₂ – 415 elliptical planform hydrofoil. This was done primarily to investigate the 3D ability of the solver. The results are validated with experimental data. Special focus is given to tip vortex strength and lift variation as a function of cavitation number. Both are well predicted.

1 Introduction

Cavitating flows occur in nearly all hydraulic machinery. Performance of different applications such as submarine propulsion and hydropower turbines are affected by cavitation. Cavitation from submarine propellers generate unwanted noise, while hydro turbine cavitation causes enormous yearly maintenance costs for the hydropower industry.

Numerical modeling of cavitation has, until recently, only been possible using cutting edge in-house CFD codes. Special challenges occur since cavitating flows are highly dynamic in nature. Also, such flows are characterized by large gradients in the density field, which is known to cause numerical instabilities.

With the release of the CFD solver Fluent 5, a cavitation model is available with a general-purpose commercial software package. Fluent 5 is a finite volume based solver that fully supports unstructured multiblock meshes. The cavitation model shipped with Fluent 5 is essentially based on the paper by Kubota *et al.* (1992). This paper is meant as a reference for validation of the cavitation model in Fluent 5. The software will, in later studies, be used to enhance the understanding of the cavitation phenomenon.

2 The Fluent 5 Cavitation model

The flow solution procedure in Fluent 5 is the SIMPLE routine presented by Patankar & Spalding (1972). This solution method is designed for incompressible flows, thus being implicit. The full Navier Stokes equations are solved. The cavitation model itself is highly physical utilizing the Rayleigh–Plesset equation to calculate bubble growth and collapse, while a volume of fluid model (VOF) is implemented to track the

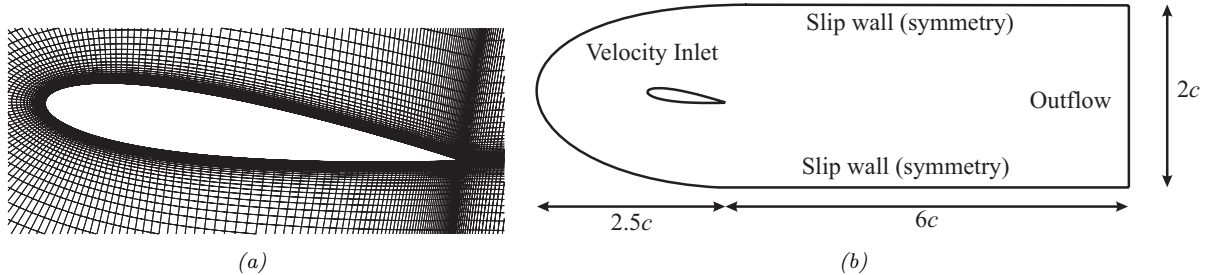


Figure 1: Figure a) shows a grid closeup surrounding the 2D hydrofoil. The grid is a C-type grid. Figure b) shows an outline of the computational domain with boundary condition type showing. The figures show the foil at 8 degrees angle of attack.

resulting void fraction field. The VOF model is based on equation 1, and will when solved along with the flow equations, give the void fraction at any solution point in the computational domain.

$$\frac{\partial \alpha}{\partial t} + \frac{\partial(\alpha u)}{\partial x} + \frac{\partial(\alpha v)}{\partial y} = \frac{D\alpha}{Dt} = \frac{1}{\rho_g} \left(\dot{m}_{lg} - \frac{d\rho}{dt} \right) \quad (1)$$

Here α is the void fraction and \dot{m}_{lg} is the mass transfer rate from liquid to gas per unit volume. The terms on the right hand side of this equation describes the phase change in the system. To be able to solve this, the mass transfer rate has to be calculated, which is done with a simplified Rayleigh–Plesset equation given as equation 2. This expression can easily be derived by neglecting the higher order terms of the original Rayleigh–Plesset equation.

$$\frac{dR}{dt} = \sqrt{\frac{2(p_v - p)}{3\rho_L}} \quad (2)$$

The cavitation model implemented in the version of Fluent that was used in this study (version 5.1.18) does not explicitly calculate bubble collapse. The solution will, however, still yield information of cavity boundaries.¹

The cavitation model suffers from several simplifications, where the most critical is probably that both phases has to be treated as incompressible. Similar calculations by Song *et al.* (1997) indicates that the compressibility of the vapor phase is important.

3 Numerical Implementation

3.1 Geometry and Grid

The 2D geometry was made to resemble the test section of the high speed water tunnel at the Saint Anthony Falls laboratory in Minneapolis, MN (SAFL). The chord length of the foil is 81mm and the domain stretches 2.5 chord lengths upstream and 6 chord lengths downstream measured from the trailing edge. Simulations for 8 and 6 degrees angle of attack are presented. In the direction from the upper and lower foil surface, the computational domain stretches one chord length in both directions. The lengths are chosen from the test section in the water tunnel and the purpose of the calculations is to reproduce experiments. Test calculations show that the blockage effect is negligible for the SAFL tunnel set-up.

Figure 1(a) shows a closeup of the 2D grid at 8 degrees angle of attack. The grid is a C-grid type with a total of about 29000 cells. The smallest cell size in the direction from the wall is 0.01mm, which corresponds to approximately $1/100 \cdot \text{Re}^{-1/2}$. This results in the first grid point being at $y^+ < 3$ on both surfaces.

In the 3D case, the main challenge was to generate a proper grid. The calculations were set up to resemble experiments taken from a paper by Arndt & Keller (1992). The foil is an elliptical planform NACA 66₂ – 415 that is mounted in a water tunnel. In the spanwise direction, the foil stretches about halfway through the test section. A detailed description of the shape of the hydrofoil can be found in Arndt & Keller (1992).

¹The latest version of Fluent ships with a more sophisticated cavitation model that explicitly calculates bubble collapse

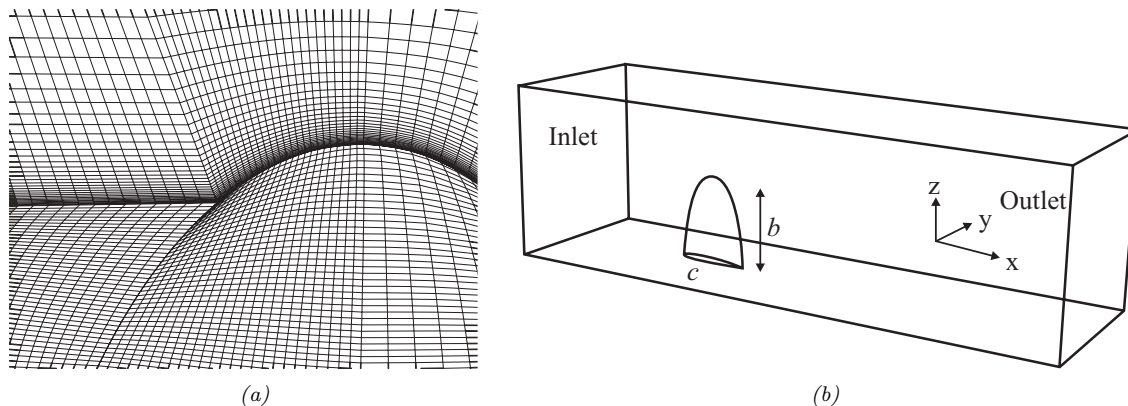


Figure 2: Figure a) shows the surface grid at the foil. The grid is denser at the tip of the foil to resolve the forming tip vortex. Figure b) shows an outline of the computational domain.

The geometric singularity at the termination point of the ellipse main axis was avoided by making the final airfoil shape to be drawn approximately 0.1mm in chord length. Implicitly the location will be very close to an analytical geometric singularity. To properly resolve the vortex that is forming at the tip of the foil, a grid of at least 15 grid points across the vortex core is needed, see Dacles-Mariani *et al.* (1995). The problem is that the path of the vortex core is not known exactly prior to the calculations. In this study an iterative approach was used to accurately place the finer grid in the vortex core. First a crude calculation was performed, to locate the general shape of the vortex. Then, by investigating the solution, the grid was refined in the center of the vortex. This was done a total of three times, each iteration refining the grid in the vortex region. Furthermore, test calculations showed that the grid-cell layer closest to the foil surface has to be small to accurately calculate lift data. This means that the viscous boundary layer has to be resolved at the complete foil surface. The grid type was structured, where the total computational domain were split in 16 different gridding blocks. The total grid size was in excess of half a million cells. A picture of the foil surface grid and the computational domain is shown in Figure 2(a) and Figure 2(b).

3.2 Boundary Conditions

Figure 1(b) shows the total 2D computational domain with lengths and boundary conditions showing. The inlet boundary condition is specified velocity, using a constant velocity profile. Upper and lower boundaries are slip walls, i.e. a symmetry condition. The outlet used is a constant pressure boundary condition. The foil itself is no-slip wall. The inlet is set to 10m/s which corresponds to a Reynolds number equal to $1.2 \cdot 10^6$ based on chord length. This is in the same range as the experimental data. The same boundary conditions are used for the 3D case. The computational domain stretches 2 chord lengths upstream and 6 chord lengths downstream.

3.3 Numerical method

The solving strategy used is the unsteady SIMPLE algorithm, Patankar & Spalding (1972). The convective flow terms are discretized using second order upwind schemes. This is also used for the Volume of Fluid equation and the Rayleigh–Plesset equation. The pressure is discretized using a second order central scheme. The implicit time formulation used is also of second order accuracy. Internally, all numbers are stored and calculated with double precision. The time step used was 0.0001s . This gives 20-30 time steps per cycle as calculated using a Strouhal number of 0.2, using the maximum foil thickness as a reference length. This time step is equivalent to a sampling frequency of 10kHz . The cavitation model itself was configured with a nuclei density of $200000 \cdot 1/\text{m}^3$. This number is 20 times higher than the value suggested by Kubota *et al.* (1992). However, the nuclei density was measured in the SAFL test tunnel to be within the chosen range. It is believed that increasing the nuclei density in the numerical model will increase the dynamics of the system, thus adding instability, however this was not a problem in this study. The water vapor pressure,

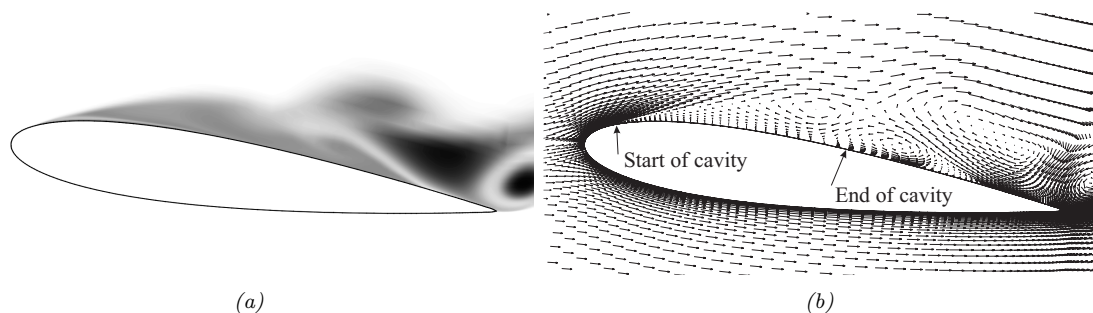


Figure 3: Figure a) shows a constant pressure contour plot for $\sigma/2\alpha = 5$ at 8 degrees AoA. Figure b) shows the corresponding velocity vector plot. Both plots are instantaneous and at the same time.

p_v , was set to 2400Pa. The cavitation number was adjusted by changing the reference pressure, P_{ref} , in the solver. The same effect can also be achieved by having a constant reference pressure and adjusting the vapor pressure. The solver parameters used are the same for both the 2D and the 3D calculations.

3.4 Turbulence modeling

A main part of this study was to validate the codes ability to capture the dynamic behavior of cavitating flows. In this study experience has shown that the normal Reynolds-averaged Navier–Stokes (RANS) based turbulence models are not suited for dynamic calculations. The time-averaging involved will smooth out time dependant turbulent phenomena. Test calculations showed this clearly were the solution simply converged to a steady state. In the 3D case, a RANS model dramatically increased the diffusion of the vortex core, thus the minimum pressure inside the vortex is not correctly predicted. The current version of Fluent 5 can not combine the Large Eddy Scale turbulence model (LES) with the cavitation model. Therefore, a plain Navier–Stokes solver was used with no turbulence modeling at all. It is expected that dynamic features like lift oscillations will tend to have higher amplitudes than measured values when using a plain Navier–Stokes solver. This can be explained by the lack of turbulent energy dissipation modeling.

4 Results

4.1 2D NACA 0015 Hydrofoil

An important parameter in cavitating flows is the cavity length. Experimentally, this is determined by analysis of high speed movies. The cavity length will generally vary a lot during a cycle, thus an average value is plotted. The same technique is used in the numerical approach, where a combination of velocity vector plots, and contours of constant vapor fraction plots are analyzed. An example of an instantaneous contour plot and velocity vector plot at the same instant in time is shown in figure 3. Here we can see that the cavity length is not easily identified from the contour plot alone, while the velocity vector plot clearly shows the reentrant jet and the closure of the attached cavity. Note that these pictures are instantaneous. Very strong vortex structures downstream of the cavity gives very low pressure regions that effectively transports the bubbles that are shed from the foil. The cavity length for a flat plate at an angle of attack, α , was shown to scale with the composite parameter, $\sigma/2\alpha$ by Acosta (1955). Arndt (1981) suggested the use of this parameter for thin hydrofoils. The cavity length, l , is normalized with respect to chord length, c , and plotted versus the parameter $\sigma/2\alpha$. In Figure 4, the numerical results are plotted with the corresponding experimental results. As we can see, the code can predict the cavity length with high accuracy. Although the current Fluent code does not have a physical correct model for calculating bubble collapse, the accurate prediction of the cavity length can still be explained. The reentrant jet will transport liquid phase into the cavitating regime at the end of the cavity. Visually, this will result in a closure of the cavity in a phase contour plot. It is also worth mentioning that the cavity length alone does not describe the flow. This can be seen clearly from the contour of constant void fraction plots shown in Figure 5. Both pictures are from $\sigma/2\alpha = 7$ but different angles of attack. The cavity length is the same, but the flow is very different. At

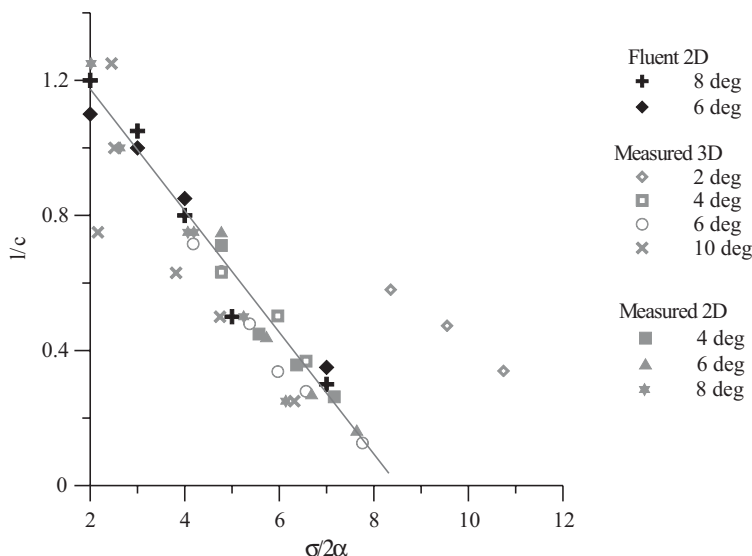


Figure 4: Cavity length plotted as a function of $\sigma/2\alpha$. The length is normalized with respect to chord length. The 3D and 2D data is collapsed by scaling the angle of attack with the aspect ratio, A , such that $\alpha_{2D} = \alpha_{3D} \cdot A/(A + 2)$. The anomaly found for 2 degrees AoA in the experimental 3D case is explained by the presence of bubble cavitation instead of sheet cavitation

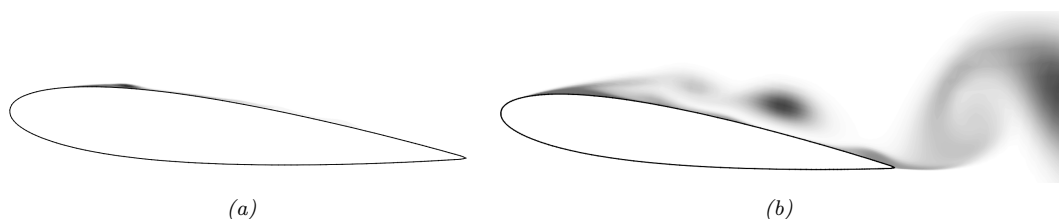


Figure 5: Figure a) shows a contour plot of constant water vapor for 6 degrees AoA and Figure b) shows a corresponding plot for 8 degrees AoA. Both plots are typical instantaneous snapshots of the flow. In both cases $\sigma/2\alpha = 7$.

8 degrees angle of attack, the flow is much more violent with large structures shedding of the suction side while the 6 degrees case is practically stable.

Kjeldsen *et al.* (2000) shows that the flow over this hydrofoil passes through several cavitation regimes ranging from inception to supercavitating. The same sequence of cavitation regimes are found in the numerical model as reported from the experiments. It must be emphasized that the difference between patch and bubble cavitation as reported by Fluent, is determined based on whether the patch sheds itself (bubble cavitation) or is sustained for a certain period of time. The determination of the cavitation regimes was done by visual inspection of contour plots of the numerical solution.

In engineering applications, prediction of lift breakdown is important. This was also calculated and compared to experimental results. The lift is oscillating with different amplitudes at different cavitation numbers. The lift fluctuates with largest amplitudes when the cavity length is about 0.75 chord lengths, corresponding to $\sigma/2\alpha$ of about 4. Experimental results are not available for 8 or 6 degrees angle of attack, and the lift does not seem to scale with the parameter $\sigma/2\alpha$. The general shape of the lift breakdown curve can still be compared. The results are plotted in Figure 6(a). The cavitation model does not seem to capture the distinct breakdown that is measured. It is believed that this is caused by the lack of compressibility in the vapor phase, i.e. the flow that is closest to the suction side in the foil.

The last parameter that is presented in this study is shedding frequency measured from lift fluctuations. Experimentally, several trends have been found for this phenomenon. The shedding frequencies has been calculated with the use of FFT's of the lift data. Experimentally, the shedding frequencies has been estab-

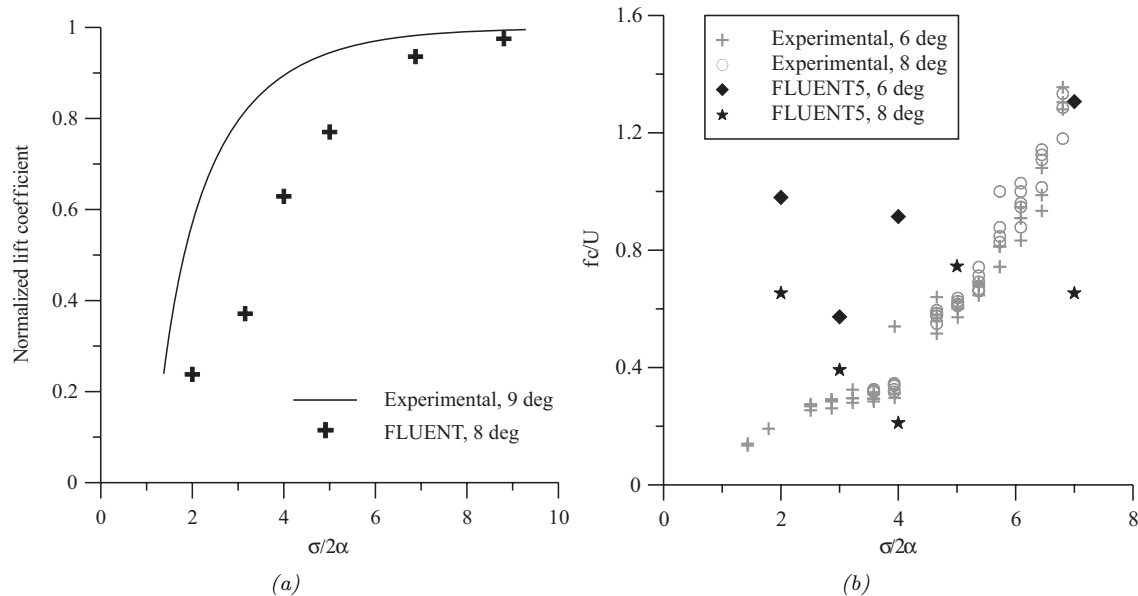


Figure 6: Figure a) shows normalized lift as a function of $\sigma/2\alpha$. Figure b) shows Strouhal number as a function of $\sigma/2\alpha$.

lished by counting frames in high speed movies or by spectral analysis of lift/pressure dynamics, Kjeldsen *et al.* (2000). The compared results are plotted in Figure 6(b). The computed results are not very accurate as they do not show any signs of trends, which are clearly present in the experimental data.

4.2 3D NACA 66₂ – 415 Hydrofoil

The 3D case is much more complicated. Also, not very much validation data is available. A study by Arndt & Keller (1992) measured lift distributions as a function of cavitation number and other flow characteristics like tip vortex strength. This data were used for comparison. The experiments were performed at St. Anthony Falls laboratory, University of Minnesota and Versuchsanstalt für Wasserbau (VW), Technical University of Munich.

It was clear that to properly calculate cavitation in this 3D configuration, it was absolutely imperative to get a correct vortex strength. The pressure inside the tip vortex is the lowest in the computational domain if the vortex strength is correct, thus this is the first location that cavitation will occur. Figure 7(a) shows the calculated vortex strength compared with experimental. The shape of the vortex is very well captured with the CFD code. The extension of the vortex core are the same in both calculations and those measured. The outer regions of the vortex are also captured well, and note that the vortex originating from shedding off the suction side is also represented. It should at this point be mentioned that the results from Fluent are taken at one discrete time-step, while the measurements are based on time averaging. The "ripple" in the z-velocity distribution wasn't found until after the refinement on the foil surface grid was made to properly resolve the boundary layer. Figure 8 shows a constant pressure contour plot with the suction side of the foil visible. The tip vortex path is visualized as a low pressure region stretching from the tip of the foil and downstream. Although, not quantified, it was noticed that the vortex core precesses slightly around its mean centerline. This behavior is also observed and described in experimental papers, Fruman *et al.* (1994)

The appearance of developed cavitation on the bulk part of the foil will decrease the lift dramatically. When lift, and hence blade loading, vanish, the source for tip vortex cavitation will diminish. A good agreement between the numerical works and the experiments can be seen, Figure 7(b). A remark to be given is that cavitation also produces unsteadiness in lift in this case. These dynamics has been proven to be a major issue, and has been demonstrated by e.g. Kjeldsen *et al.* (2000) experimentally on the same 2D NACA0015 hydrofoil used for the 2D calculations in this paper. The lift measurements from VW are time averaged, the numerical works are averaging lift when supposedly steady oscillatory conditions are monitored.

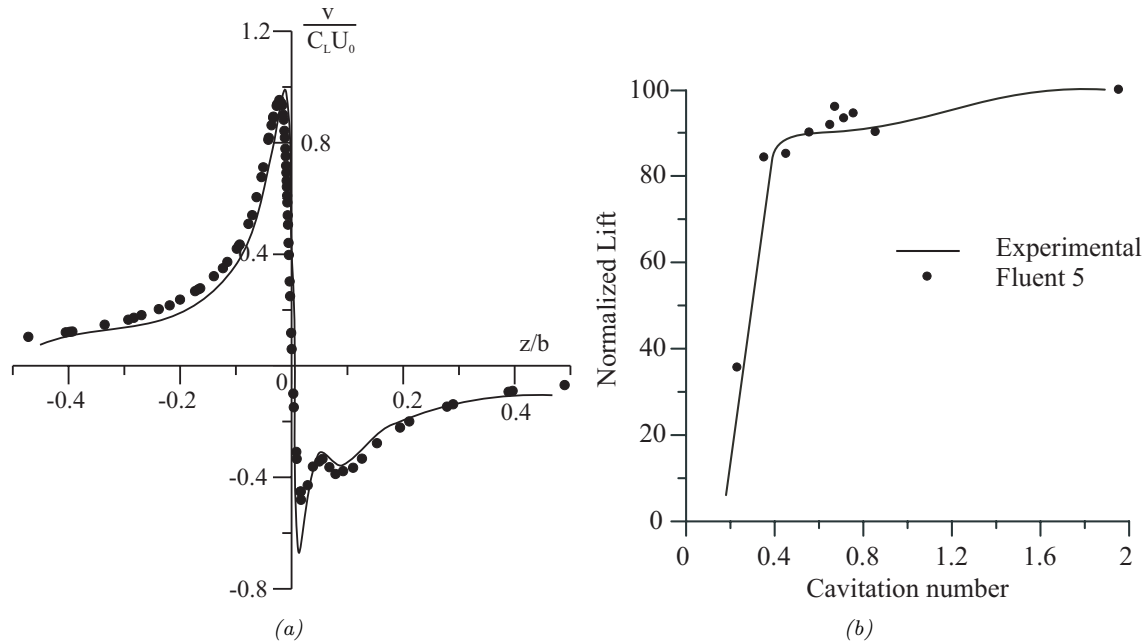


Figure 7: Figure a) shows tip vortex strength one chord length downstream of trailing edge. The vertical velocity, v , is normalized with respect to lift coefficient, C_L , and free stream velocity, U_0 . The z -direction is normalized with respect to the total height of the hydrofoil. Figure b) shows a contour plot of constant pressure, visualizing the shape of the vortex stretching from the hydrofoil tip. The flow is from right to left.



Figure 8: Contour plot of constant pressure visualizing the shape of the vortex stretching downstream from the hydrofoil tip. The flow is from right to left. The low pressure regions close to the trailing edge is caused by shedding from the suction side of the foil.

The averaging was however only made over a few cycles due to time limitations in actual computing time.

5 Conclusions

In general, the results are very promising. Several aspects of cavitation can be accurately captured with the current cavitation model. Visually, the flow is very well predicted. Especially, the cavity length can be calculated with a high degree of accuracy. This is an important feature in engineering aspects, since cavity collapse close to surfaces will cause damage. Also, with this code, it is easy to quantitatively adjust the overall cavitation number in the computational domain accurately. This is demonstrated by the good agreement between cavitation regimes and cavity length from experimental data and the numerical data respectively. Both in the 3D and the 2D cases, the different cavitation regimes were found to match the reported experimental data.

The dynamics of the system is still not very accurately calculated. The model suffers from several assumptions which most likely cause this. The numerically calculated Strouhal numbers does not show any distinct trends, while this is clearly present in the experimental data. On the other hand, all calculated frequencies are in the same order of magnitude as the experimental data. System dynamics were only investigated for the 2D calculations.

Lift characteristics is fairly well calculated and the 3D case is actually better than the corresponding 2D case. The distinct breakdown in lift when the cavitation number reaches a certain point is observed in the 3D case while the 2D simulations does not show this feature. Instead, the lift seems to drop in a more gradual manner. The calculations are still within reasonable accuracy.

Acknowledgments

The authors would like to thank the Supercomputer Institute at the University of Minnesota for computer time and kind technical support.

References

- ACOSTA, A. J. 1955 A note on partial cavitation of flat plae hydrofoils. *Tech. Rep.* E-19.9. California Institute of Technology.
- ARNDT, R. E. A. 1981 Recent advances in cavitation research. *Advances in Hydroscience* **12**.
- ARNDT, R. E. A. & KELLER, A. 1992 Water quality effects on cavitation inception in a trailing vortex. *ASME, Journal of Fluids Engineering* **114**, 430–438.
- DACLES-MARIANI, J., ROGERS, S., KWAK, D., ZILLIA, G. & CHOW, J. S. 1995 Numerical/experiental study of a wingtip vortex in the near field. *AIAA Journal* **33** (9), 1561–1568.
- FRUMAN, D. H., CASTRO, F., PAUCHET, A. & PICHON, T. 1994 On tip vortex turbulence, wandering and cavitation occurence. The Second International Symposium on Cavitation, Tokyo, Japan.
- KJELDSSEN, M., ARNDT, R. E. A. & EFFERTZ, M. 2000 Spectral characteristics of sheet/cloud cavitation. *ASME, Journal of Fluids Engineering* **122**, 481–487.
- KUBOTA, A., KATO, H. & YAMAGUCHI, H. 1992 A new modeling of cavitating flows: a numerical study of unsteady, cavitation on a hydrofoil section. *Journal of Fluid Mechanics* **240**, 59–69.
- PATANKAR, S. V. & SPALDING, D. B. 1972 A calcuation procedure for heat, mass and momentum transfer in three-dimensional parabolic flows. *International Journal of Heat and Mass Transfer* **15**, 1787+.
- SONG, C. C. S., HE, J., ZHOU, F. & WANG, G. 1997 Numerical simulation of cavitating and non-cavitating flows over a hydrofoil. *Tech. Rep.* 402. University of Minnesota, St. Anthony Falls Laboratory.